



Interglacial Antarctic–Southern Ocean climate decoupling due to moisture source area shifts

A. Landais^{1,9}✉, B. Stenni^{2,9}, V. Masson-Delmotte¹, J. Jouzel¹, A. Cauquoin³, E. Fourré¹, B. Minster¹, E. Selmo⁴, T. Extier^{1,8}, M. Werner⁵, F. Vimeux^{1,6}, R. Uemura⁷, I. Crotti^{1,2} and A. Grisart¹

Succession of cold glacials and warm interglacials during the Quaternary results from large global climate responses to variable orbital configurations, accompanied by fluctuating greenhouse gas concentrations. Despite the influences of sea ice and atmospheric and ocean circulations in the Southern Ocean on atmospheric CO₂ concentrations and climate, past changes in this region remain poorly documented. Here, we present the 800 ka deuterium excess record from the East Antarctica EPICA Dome C ice core, tracking sea surface temperature in evaporative regions of the Indian sector of the Southern Ocean from which moisture precipitated in East Antarctica is derived. We find that low obliquity leads to surface warming in evaporative moisture source regions during each glacial inception, although this relative temperature increase is counterbalanced by global cooling during glacial maxima. Links between the two regions during interglacials depends on the existence of a temperature maximum at the interglacial onset. In its absence, temperature maxima in the evaporative moisture source regions and in East Antarctica were synchronous. For the other interglacials, temperature maxima in the source areas lag early local temperature maxima by several thousand years, probably because of a change in the position of the evaporative source areas.

The last Intergovernmental Panel on Climate Change *Special Report on the Ocean and Cryosphere in a Changing Climate*¹ has stressed the key role of the Southern Ocean for global carbon and heat uptake during the ongoing human-induced warming. This region of the world has, however, long been overlooked due to logistical challenges, leading to gaps in our understanding of past, present and future global climate change. In particular, gaps have been identified for reconstructions of past Southern Ocean changes while developing global palaeoclimate syntheses².

Recent efforts have produced data syntheses for the last deglaciation^{3,4}, which is the most documented and associated with the best chronological framework. Transient climate simulations show that the first-order deglacial climatic signal can be reproduced in Antarctica and in the Southern Ocean despite some model–proxy mismatches when looking at the timing and duration of millennial events^{5,6}. Regional differences in the climatic evolution of Antarctica and the Southern Ocean⁷, captured only partly in these simulations⁵, can help understand the driving mechanisms of deglaciations. As a first example, in response to local summer insolation, the temperature reconstruction from the West Antarctica Ice Sheet Divide ice core shows an early warming by 2 thousand years ago (ka) in West Antarctica compared with the onset of the warming in East Antarctica, the rise of atmospheric CO₂ concentration and the decrease of the northern ice-sheet volume⁸. As a second example, precise dating of deep sea sediment core shows that changes in the Southern Ocean circulation and in the East Antarctic climate were synchronous over the last deglaciation⁹. This result supports the

hypotheses of a shift of westerlies, oceanic circulation and/or productivity in the Southern Ocean as drivers of the CO₂ atmospheric concentration increase¹⁰.

Different deglacial patterns over the past 800 ka

While the picture of the succession of events (changes in orbital parameters, ice-sheet size, CO₂ concentration, temperature at different latitudes and so on) has become increasingly clear for the last deglaciation (Termination I), there is a growing interest to compare this sequence of events with those corresponding to the preceding deglaciations. Indeed, each deglaciation occurs in a different orbital context, some of the deglaciations being associated with a strong precession minimum (for example, Termination II, 130 ka) and others occurring in a low eccentricity context (for example, Termination V, 440 ka). Moreover, Termination I is remarkable for the occurrence of the Younger Dryas period in the middle of the deglacial phase. Millennial-scale events associated with modifications of the Atlantic meridional overturning circulation, iceberg discharge events, shifts of the intertropical convergence zone and bipolar seesaw behaviour leading to asynchronous temperature evolutions in the North Atlantic and Antarctic regions have also been documented during older terminations^{11,12}. Deglaciations older than Termination V (430 ka) also have a smaller amplitude, that is, leading to cooler interglacials than most recent ones¹³. Recent studies have highlighted the role of precession, CO₂ concentration, ice-sheet volume and integrated summer energy at 65°N for the onset and timing of terminations; however, many questions remain

¹Laboratoire des Sciences du Climat et de l'Environnement, LSCE/IPSL, CEA-CNRS-UVSQ, Université Paris-Saclay, Gif-sur-Yvette, France. ²Department of Environmental Sciences, Informatics and Statistics, Ca' Foscari University of Venice, Venezia, Italy. ³Institute of Industrial Science, The University of Tokyo, Kashiwa, Japan. ⁴Department of Chemistry, Life Sciences and Environmental Sustainability, University of Parma, Parco Area delle Scienze, Parma, Italy. ⁵Alfred Wegener Institute, Helmholtz Centre for Marine and Polar Research, Bremerhaven, Germany. ⁶HydroSciences Montpellier (HSM), UMR 5569 (UM, CNRS, IRD), Montpellier, France. ⁷Department of Earth and Environmental Sciences, Graduate School of Environmental Studies, Nagoya University, Furo-cho, Chikusa-ku, Nagoya, Japan. ⁸Present address: EPOC, UMR 5805, CNRS, Université de Bordeaux, Pessac, France. ⁹These authors contributed equally: A. Landais, B. Stenni. ✉e-mail: amaelle.landais@lsce.ipsl.fr

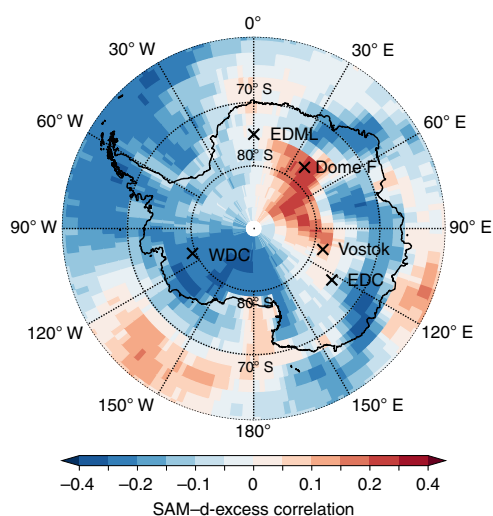


Fig. 1 | Modelled correlation between d-excess and SAM. The correlation has been obtained using the ECHAM6-wiso model over 30 years in a pre-industrial run, and we have indicated the positions of five Antarctic ice cores on the map (WDC, West Antarctica Ice Sheet Divide core; EDML, EPICA Dronning Maud Land).

open to explain the variety of triggering conditions and regional climatic signals over the different deglaciations^{11,14}.

In this study, we address the link between Antarctic temperature records and climatic variability at lower latitudes, mainly in the Southern Ocean, using water isotope records spanning the last nine deglaciations. For this aim, we combine new δD and $\delta^{18}O$ measurements from the 800 ka EPICA (European Project for Ice Coring in Antarctica) Dome C (EDC) ice core to produce the longest ice-core record of deuterium excess (d-excess), defined as $\delta D - 8 \times \delta^{18}O$ ¹⁵ (Methods). The d-excess is a classical ice-core tracer of climate conditions in the low-latitude regions of moisture evaporation¹⁶. The d-excess is very sensitive to relative humidity at evaporation over the ocean because of different sensitivities of δD and $\delta^{18}O$ to kinetic and equilibrium fractionation^{17,18}. Because the equilibrium fractionation factors associated with $\delta^{18}O$ and δD show different sensitivities to temperature, d-excess is also largely influenced by the temperature difference between the source evaporative region and the site of precipitation.

The d-excess and associated source evaporative region temperature have already been investigated in several deep Antarctic ice cores covering several glacial–interglacial cycles (Vostok over the past 400 ka, Dome F over the past 720 ka, Fig. 1), showing a strong influence of the obliquity signal on the temperature of the source evaporative regions^{16,19,20}. Yet climatic reconstructions from the Vostok and Dome F ice cores show substantial differences, mainly during deglaciations, with a larger and more rapid source temperature increase for Dome F than for Vostok, suggesting either regional variability of deglacial changes in the Southern Ocean or artefacts in the climate reconstruction using Antarctic d-excess records²¹. In this article, we show that the EDC d-excess record is probably less affected by these artefacts. This makes EDC d-excess a faithful tracer for the reconstruction of climatic conditions of the source evaporative regions for precipitation reaching the Dome C area. It is hence used to provide the Antarctica versus Indian Ocean sector of the Southern Ocean pattern of deglaciations.

Climate reconstruction of the source evaporative regions

The 800 ka d-excess record (Fig. 2 and Extended Data Fig. 1) from EDC depicts orbital variability already visible in the δD record: d-excess displays maxima during interglacial periods and minima

during glacial maxima. Still, the d-excess increases over deglaciations are often occurring on longer time intervals than the δD increases. As an example, during Termination III, the d-excess increase lasts more than 15 ka while the δD increase lasts less than 10 ka. The d-excess generally peaks with minimum in obliquity, especially at the onset of glacial periods^{16,20}. Despite first-order similarities in the d-excess profiles at EDC, Vostok and Dome F, important differences are visible. There is first a higher average d-excess over the last 400 ka at Dome F and Vostok (respectively, $13.9 \pm 3.1\text{‰}$ and $15 \pm 1.4\text{‰}$) compared with EDC ($7.7 \pm 1.8\text{‰}$). Then we observe a different timing of the d-excess maxima, especially between Dome F and EDC (for example, 5 ka over Termination I, 10 ka over Termination VII), a difference that cannot be explained by chronology issues since all records are displayed on the consistent AICC2012 chronology²². The difference in average d-excess is directly linked to the lower $\delta^{18}O$ values at Dome F and Vostok than at Dome C due to the longer distillation path to reach Dome F and Vostok than EDC. The different timing of maxima calls for more in-depth investigations of climatic interpretation of d-excess, including regional effects.

In remote regions of the East Antarctic plateau, d-excess is influenced by local temperature so that d-excess is generally strongly anticorrelated with $\delta^{18}O$ in surface snow and precipitations when $\delta^{18}O$ values are below -40‰ ^{18,23,24}. An alternative definition has been proposed to remove this effect at Dome F, $d_{in} = 1,000 \times \ln(1 + \delta D) + 2.85 \cdot 10^{-2} \times (1,000 \times \ln(1 + \delta^{18}O))^2 - 8.47 \times 1,000 \times \ln(1 + \delta^{18}O)$ ^{21,25}, which can also be applied to the other East Antarctica sites (Methods and Extended Data Figs. 2 and 3).

On the basis of calibrations performed with isotopic models, past changes in temperature are reconstructed at precipitation sites (T_{site}) and at source evaporative regions (T_{source}) using $\delta^{18}O$ and δD variations at our three Antarctic sites^{21,26,27} (Methods). The T_{site} reconstructions are very close to the δD and $\delta^{18}O$ records for EDC, Vostok and Dome F and are very coherent between the three sites (Fig. 2). By contrast, the T_{source} d-excess and d_{in} signals exhibit substantial differences between the three sites (Fig. 2 and Extended Data Fig. 4), suggesting either regional differences or biases when calculating T_{source} from d-excess or d_{in} . At EDC, the T_{source} signal is strongly correlated with either d_{in} or d-excess ($R = 0.93$), both being strongly correlated ($R = 0.80$). The similarity of the T_{source} d-excess and d_{in} signals at EDC over the past 800 ka supports the fact that the EDC excess signal (d_{in} or d-excess) is straightforward to be interpreted in terms of T_{source} . This result contrasts with the different relative evolutions of Vostok and Dome F T_{source} d-excess and d_{in} , d-excess and d_{in} being less correlated than at EDC ($R < 0.6$, Extended Data Table 1).

An alternative possibility to interpret d-excess or d_{in} in terms of climate parameters avoiding calculation of T_{source} is to use outputs of simulations obtained with atmospheric general circulation models or coupled global climate models equipped with water isotopes^{28,29}. Using the Goddard Institute for Space Studies (GISS) model ($4^\circ \times 5^\circ$ resolution) equipped with isotopes in a pre-industrial control run, Schmidt et al.²⁹ showed that the d-excess over the whole East Antarctic plateau is anticorrelated with the Southern Annular Mode (SAM, the leading mode of variability in the Southern Hemisphere atmospheric circulation), a behaviour explained by the northward shift of the Southern Hemisphere westerlies during the negative SAM phase. This result was later used to interpret variations of d-excess over the last glacial period³⁰. The SAM variability and amplitude were, however, probably different in the past³¹, and we thus do not aim at interpreting past d-excess signal in term of SAM.

Here we examine regional variability of the d-excess and d_{in} signals using the most recent high-resolution ECHAM6-wiso model at 1.875° resolution³². The performances of this model for water isotopic variability in Antarctica and SAM representation have been well evaluated (Methods and Extended Data Figs. 5–8). In the pre-industrial ECHAM6-wiso free simulation, the link between d-excess and SAM is different from one site to the others, which

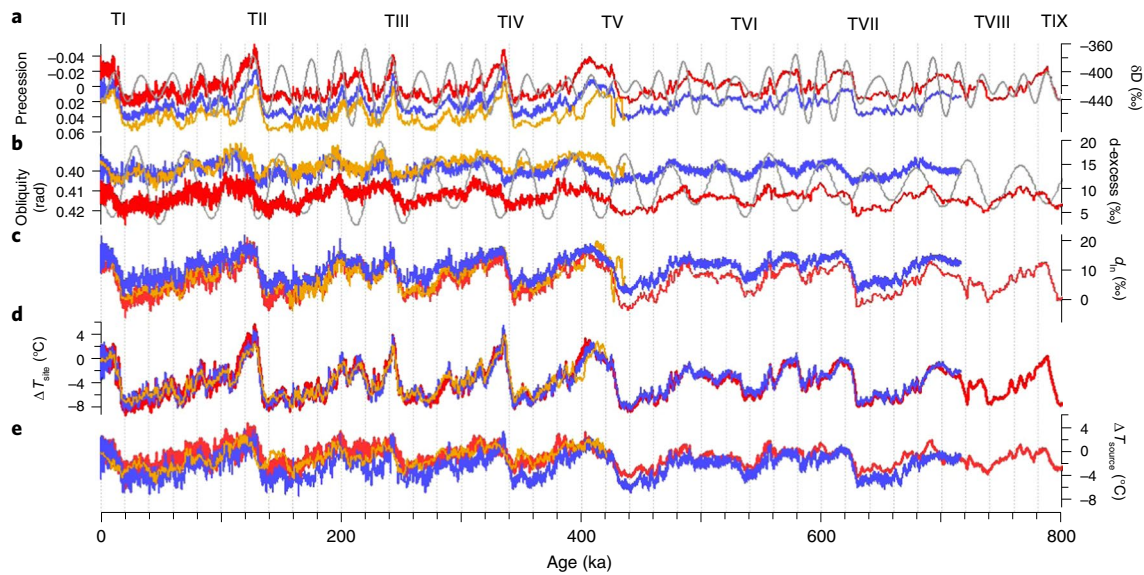


Fig. 2 | Water isotopic series and climate reconstruction from three deep ice cores in East Antarctica. a–e, δD (a), d-excess (b), d_{in} (c), ΔT_{site} (d) and ΔT_{source} (e) series from the EDC (red), Dome F (blue) and Vostok (orange) ice cores (Δ stands for variation with respect to present-day values). Precession (a, inverse scale) and obliquity (b, inverse scale) are shown in grey. The numbering of the glacial terminations is also displayed (Termination I (TI) is the last deglaciation and TIX the oldest one recorded in available Antarctic ice cores).

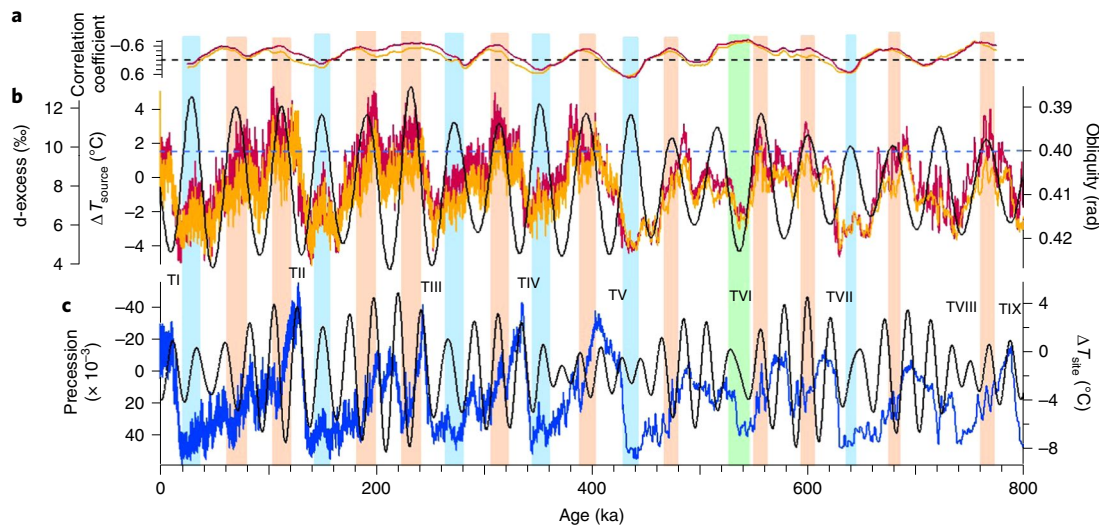


Fig. 3 | Link between ΔT_{source} , d-excess, ΔT_{site} and orbital parameters. a, Correlation coefficient between obliquity and ΔT_{source} (orange) and between obliquity and d-excess (red) over a 50 ka sliding window; the dashed black horizontal line indicates a correlation of 0. b, EDC d-excess (red), ΔT_{source} (orange) and obliquity (black). c, EDC ΔT_{site} (blue) and precession (black). The blue/orange rectangles are associated with obliquity value lower than 0.4 rad (dashed blue horizontal line) with correlation coefficient between ΔT_{source} (or d-excess) and obliquity being positive/negative. A green rectangle indicates the peculiar situation over Termination VI.

contradicts previous observations from the GISS model: d-excess is correlated with SAM at Dome F, slightly correlated with SAM at Vostok and weakly anticorrelated with SAM at EDC (Fig. 1). By contrast, d_{in} and SAM are anticorrelated over the whole East Antarctic plateau (Extended Data Fig. 9). The correlation between an ‘excess’ signal and SAM is less dependent on its definition (d-excess or d_{in}) at EDC (anticorrelation for both definitions) than at Dome F and Vostok (correlation or anticorrelation depending on the definition), supporting a more robust use of either d_{in} or d-excess to infer T_{source} reconstruction at EDC. In the following, we concentrate on the

800 ka EDC records using mostly the classical d-excess proxy for coherency with previous studies on EDC^{27,33}.

Figure 3 shows some anticorrelation between EDC d-excess and obliquity at the orbital scale as already observed for the Vostok ice core¹⁶. However, we observe large variations in the correlation coefficient. These two parameters are anticorrelated during minima of obliquity occurring at glacial inception or at a transition from a warm stage to a colder stage. By contrast, we observe a positive correlation between T_{source} and obliquity for obliquity minima occurring during strong glacial maxima (blue shaded areas). Termination VI

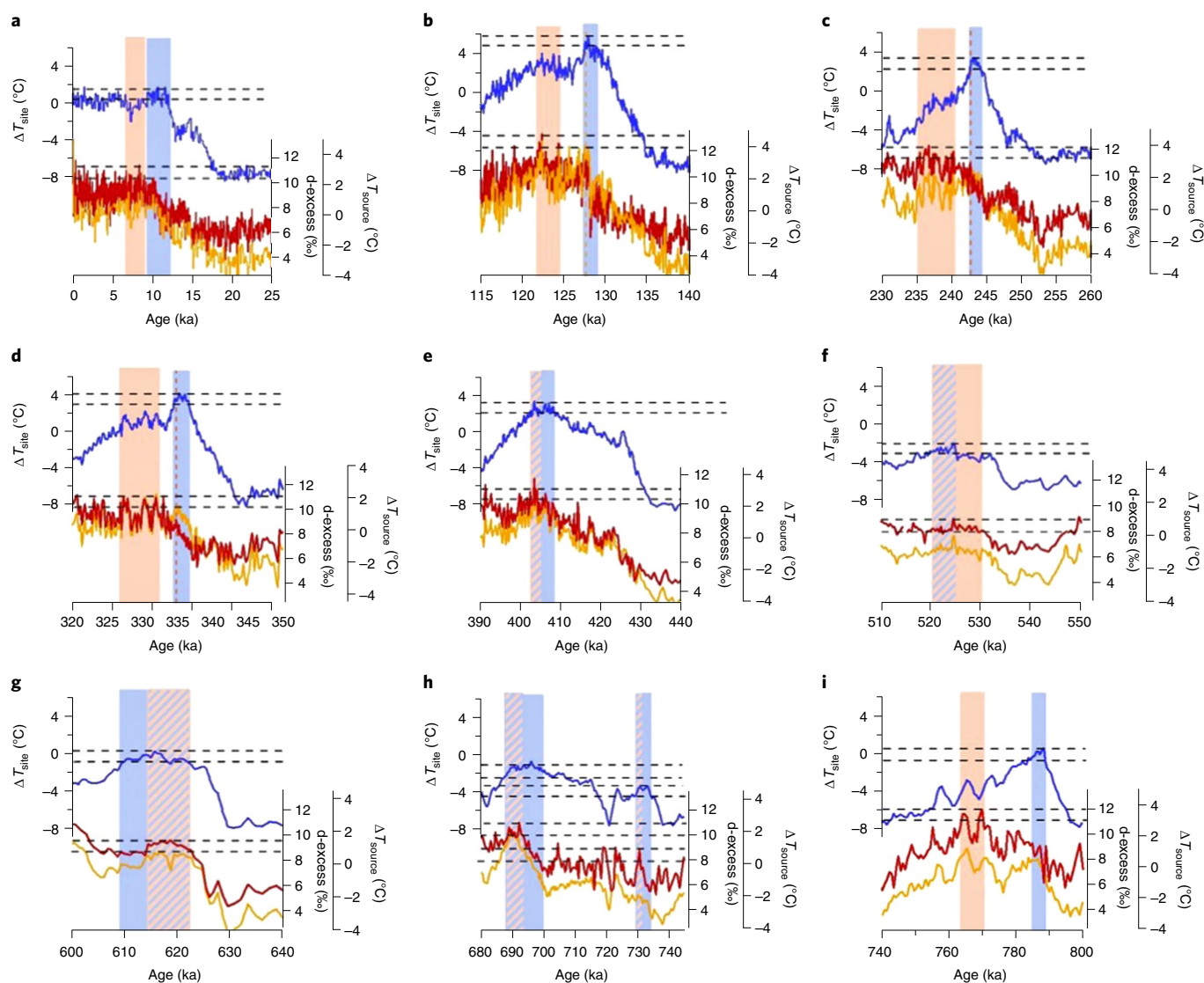


Fig. 4 | Relationship between source and site temperature over glacial termination and interglacials of the past 800 ka. Relative evolution of ΔT_{source} (orange), d-excess (red) and ΔT_{site} (blue) reconstructed from the EDC δD and $\delta^{18}O$ records over the last nine glacial terminations. **a**, Termination I. **b**, Termination II. **c**, Termination III. **d**, Termination IV. **e**, Termination V. **f**, Termination VI. **g**, Termination VII. **h**, Termination VIII. **i**, Termination IX. The vertical rectangles indicate the timing of the maximum over terminations or over interglacials for ΔT_{site} (blue) and d-excess (red). The blue rectangles include the value of the earliest ΔT_{site} maximum, and the temporal window corresponds to ΔT_{site} values less than 1°C lower (dashed horizontal lines). The orange rectangles include the earlier maximum in d-excess, and the temporal window corresponds to d-excess values less than 1‰ lower (dashed lines). When ΔT_{site} and d-excess maxima are synchronous, a blue-orange hatched rectangle is displayed. For Terminations III and IV, a vertical orange dashed line shows a first maximum seen in ΔT_{source} only (not in d-excess).

shows a peculiar behaviour with a strong anticorrelation observed at about 530 ka when obliquity is maximum (green rectangle on Fig. 3).

Southern Ocean versus Antarctica climate

Previous studies^{16,27} explained the anticorrelation between T_{source} or d-excess and obliquity as an increase (decrease) of the latitudinal temperature gradient between East Antarctica source evaporative regions (45°S on average in the Indian sector for EDC at present day³⁴) and East Antarctica sites during obliquity minima (maxima). This result characterizes an important positive feedback during glacial inceptions: a larger insolation gradient increases the temperature gradient between oceanic evaporation source regions and cooling polar regions. This leads to an increase in the amount of moisture advected to polar regions where enhanced snowfall deposition supports the growth of polar ice sheets.

Such a mechanism seems less active during glacial maxima when d-excess and T_{site} exhibit a synchronous minimum. Northward shifts of the evaporative regions in the Southern Ocean probably occurred during glacial maxima because of the combined effect of the obliquity minimum and the large extension of Antarctic sea ice: a slight local maximum in d-excess is seen during this glacial maxima. However, the dominant effect on d-excess and T_{source} is the global cooling, imprinted in both Antarctic temperature and global mean ocean temperature³⁵.

Our results illustrate the competition between the effects of global mean climate change and obliquity on the Southern Ocean climate. A reconstruction of upwelling in the austral ocean driven by southern westerly winds over the last climatic cycle has indeed shown that while low obliquity during glacial inception leads to a strengthening of the westerlies because of stronger latitudinal gradient, the global

warming during the deglaciation leads to poleward shift of the westerlies counteracting the effect of increasing obliquity³⁶.

When looking in more details at the d-excess versus T_{site} evolutions over the last nine deglaciations (Fig. 4), we observe that after the concomitant minima during glacial maximum, there is a delay of several millennia between the maximum in T_{site} and the maximum in d-excess over more than half of the interglacial periods (Marine Isotopic Stage (MIS) 1, 5, 7, 9 and 19 corresponding to the end of Terminations I, II, III, IV and IX, respectively). EDC T_{source} and d-excess have very similar evolutions except at the end of Terminations III and IV, where an early maximum of T_{source} (not observed in the d-excess) occurs only 1 ka after the T_{site} optimum. This T_{source} signal not imprinted in d-excess arises from the influence of the rapid δD variation on T_{source} reconstruction and may not reflect a true climatic signal in the Southern Ocean.

Unlike what is observed over MIS 5, 7, 9, 19 and to a lesser extent MIS 1, no delay between T_{site} and T_{source} maxima is observed over the other interglacials of the past 800 ka (that is, MIS 11, 13, 15 and 17 beginning at the end of Terminations V, VI, VII and VIII). For these last interglacial periods, the maximum in Antarctic temperature does not occur at their onset as for MIS 1, 5, 7, 9 and 19 but in the second half of the interglacial period.

Terminations I, II, III, IV and IX end with an Antarctic excess warmth¹³, a period lasting 1–2 ka with higher T_{site} than the T_{site} value of the following interglacial plateau. This Antarctic excess warmth shares similarities with Antarctic temperature evolution linked to the bipolar seesaw behaviour observed over the millennial events of the last glacial period. In particular, it has been suggested that deglaciations ending with an optimum in the Antarctic temperature have the characteristics of a millennial event initiated by a southern warming occurring in a period when large ice-sheet size prevented any early abrupt northern warming. As for the classical bipolar seesaw expression, the maximum in East Antarctic temperature at the end of these terminations is concomitant with an abrupt methane increase often associated with the late abrupt temperature increase in the Northern Hemisphere and abrupt onset of monsoon activity in South Asia³⁷. Still, while there is an almost synchronicity between the Antarctic temperature maximum and the Antarctic d-excess signal over the millennial events of the last glacial period^{30,38}, the terminations ending with an Antarctic excess warmth are followed by a continuing increase after the early maximum in T_{site} . The decoupling between δD and d-excess trends reflects a decoupling between T_{site} and T_{source} over this early interglacial millennial pattern.

The reconstruction of mean ocean temperature over the last two interglacial periods based on noble gas measurements in ice cores cannot explain this T_{site} versus T_{source} evolution since it closely resembles the evolution of the Antarctic temperature with an earlier optimum^{35,39}. We thus interpret the lack of a concomitant strong maximum in d-excess and T_{site} at the onset of the interglacial as a southward shift of the Southern Ocean evaporative regions. This shift would have attenuated the T_{source} and hence d-excess increasing signals during the Antarctic and oceanic temperature maximum. We suggest that a strong decrease of the sea-ice extent around Antarctica and modifications of the atmospheric and oceanic circulations induced by Antarctic excess warmth are the drivers of this southward shift of the moisture evaporative regions of the Indian sector of the Southern Ocean. This hypothesis is supported by previous studies showing that large decreases in sea-ice extent in the Southern Ocean connected with Antarctic warming⁴⁰ are related to shifts in atmospheric and oceanic patterns^{41,42}.

A perspective for our study is to take advantage of the increasing computing capability making it possible to run ensembles of transient simulations over different interglacials (starting or not with a strong Antarctic temperature maximum) and compare the results with the two different patterns of Antarctic versus Southern Ocean climate observed here.

Online content

Any methods, additional references, Nature Research reporting summaries, source data, extended data, supplementary information, acknowledgements, peer review information; details of author contributions and competing interests; and statements of data and code availability are available at <https://doi.org/10.1038/s41561-021-00856-4>.

Received: 16 December 2020; Accepted: 15 October 2021;

Published online: 29 November 2021

References

- IPCC *Special Report on the Ocean and Cryosphere in a Changing Climate* (eds Pörtner, H.-O. et al) (IPCC, 2019).
- Kaufman, D. et al. Holocene global mean surface temperature, a multi-method reconstruction approach. *Sci. Data* **7**, 201 (2020).
- Clark, P. U. et al. Global climate evolution during the last deglaciation. *Proc. Natl Acad. Sci. USA* **109**, E1134–E1142 (2012).
- Liu, Z., Huang, S. & Jin, Z. Breakpoint lead-lag analysis of the last deglacial climate change and atmospheric CO₂ concentration on global and hemispheric scales. *Quat. Int.* **490**, 50–59 (2018).
- Lowry, D. P., Golledge, N. R., Menviel, L. & Bertler, N. A. N. Deglacial evolution of regional Antarctic climate and Southern Ocean conditions in transient climate simulations. *Clim. Past* **15**, 189–215 (2019).
- Liu, Z. et al. Transient simulation of last deglaciation with a new mechanism for Bolling-Allerød warming. *Science* **325**, 310–314 (2009).
- Stenni, B. et al. Expression of the bipolar see-saw in Antarctic climate records during the last deglaciation. *Nat. Geosci.* **4**, 46–49 (2011).
- WAIS Divide Project Members Onset of deglacial warming in West Antarctica driven by local orbital forcing. *Nature* **500**, 440–444 (2013).
- Siani, G. et al. Carbon isotope records reveal precise timing of enhanced Southern Ocean upwelling during the last deglaciation. *Nat. Commun.* **4**, 2758 (2013).
- Menviel, L. et al. Southern Hemisphere westerlies as a driver of the early deglacial atmospheric CO₂ rise. *Nat. Commun.* **9**, 2503 (2018).
- Cheng, H. et al. The Asian monsoon over the past 640,000 years and ice age terminations. *Nature* **534**, 640–646 (2016).
- Hodell, D. A., Channell, J. E. T. & Street, D. Mode transitions in Northern Hemisphere glaciation: co-evolution of millennial and orbital variability in Quaternary climate. *Clim. Past* **12**, 1805–1828 (2016).
- Past Interglacials Working Group of PAGES Interglacials of the last 800,000 years. *Rev. Geophys.* **54**, 162–219 (2016).
- Roucoux, K. H., Shackleton, N. J., de Abreu, L., Schönfeld, J. & Tzedakis, P. C. Combined marine proxy and pollen analyses reveal rapid Iberian vegetation response to North Atlantic millennial-scale climate oscillations. *Quat. Res.* **56**, 128–132 (2001).
- Dansgaard, W. Stable isotopes in precipitation. *Tellus* **16**, 436–468 (1964).
- Vimeux, F., Masson-Delmotte, V., Jouzel, J., Stievenard, M. & Petit, J. R. Glacial-interglacial changes in ocean surface conditions in the Southern Hemisphere. *Nature* **398**, 410–413 (1999).
- Gat, J. R. Oxygen and hydrogen isotopes in the hydrologic cycle. *Annu. Rev. Earth Planet. Sci.* **24**, 225–262 (1996).
- Masson-Delmotte, V. et al. A review of Antarctic surface snow isotopic composition: observations, atmospheric circulation, and isotopic modeling. *J. Clim.* **21**, 3359–3387 (2008).
- Vimeux, F. et al. A 420,000 year deuterium excess record from East Antarctica: information on past changes in the origin of precipitation at Vostok. *J. Geophys. Res. Atmos.* **106**, 31863–31873 (2001).
- Uemura, R. et al. Asynchrony between Antarctic temperature and CO₂ associated with obliquity over the past 720,000 years. *Nat. Commun.* **9**, 961 (2018).
- Uemura, R. et al. Ranges of moisture-source temperature estimated from Antarctic ice cores stable isotope records over glacial–interglacial cycles. *Clim. Past* **8**, 1109–1125 (2012).
- Bazin, L. et al. An optimized multi-proxy, multi-site Antarctic ice and gas orbital chronology (AICC2012): 120–800 ka. *Clim. Past* **9**, 1715–1731 (2013).
- Fujita, K. & Abe, O. Stable isotopes in daily precipitation at Dome Fuji, East Antarctica. *Geophys. Res. Lett.* **33**, 6–9 (2006).
- Stenni, B. et al. Three-year monitoring of stable isotopes of precipitation at Concordia Station, East Antarctica. *Cryosphere* **10**, 2415–2428 (2016).
- Markle, B. R. et al. Global atmospheric teleconnections during Dansgaard–Oeschger events. *Nat. Geosci.* **10**, 36–40 (2016).
- Vimeux, F., Cuffey, K. M. & Jouzel, J. New insights into Southern Hemisphere temperature changes from Vostok ice cores using deuterium excess correction. *Earth Planet. Sci. Lett.* **203**, 829–843 (2002).
- Stenni, B. et al. The deuterium excess records of EPICA Dome C and Dronning Maud Land ice cores (East Antarctica). *Quat. Sci. Rev.* **29**, 146–159 (2010).

28. Werner, M., Langebroek, P. M., Carlsen, T., Herold, M. & Lohmann, G. Stable water isotopes in the ECHAM5 general circulation model: toward high-resolution isotope modeling on a global scale. *J. Geophys. Res. Atmos.* <https://doi.org/10.1029/2011JD015681> (2011).
29. Schmidt, G. A., LeGrande, A. N. & Hoffmann, G. Water isotope expressions of intrinsic and forced variability in a coupled ocean-atmosphere model. *J. Geophys. Res. Atmos.* <https://doi.org/10.1029/2006JD007781> (2007).
30. Buizert, C. et al. Abrupt ice-age shifts in southern westerly winds and Antarctic climate forced from the north. *Nature* **563**, 681–685 (2018).
31. Kim, S. J., Lü, J. & Kim, B. M. The Southern Annular Mode (SAM) in PMIP2 simulations of the last glacial maximum. *Adv. Atmos. Sci.* **31**, 863–878 (2014).
32. Cauquoin, A., Werner, M. & Lohmann, G. Water isotopes-climate relationships for the mid-Holocene and preindustrial period simulated with an isotope-enabled version of MPI-ESM. *Clim. Past* **15**, 1913–1937 (2019).
33. Stenni, B. An oceanic cold reversal during the last deglaciation. *Science* **293**, 2074–2077 (2001).
34. Winkler, R. et al. Deglaciation records of ^{17}O -excess in East Antarctica: reliable reconstruction of oceanic normalized relative humidity from coastal sites. *Clim. Past* **8**, 1–16 (2012).
35. Bereiter, B., Shackleton, S., Baggenstos, D., Kawamura, K. & Severinghaus, J. Mean global ocean temperatures during the last glacial transition. *Nature* **553**, 39–44 (2018).
36. Ai, X. E. et al. Southern Ocean upwelling, Earth's obliquity, and glacial-interglacial atmospheric CO_2 change. *Science* **370**, 1348–1352 (2020).
37. Caley, T., Malaizé, B., Kageyama, M., Landais, A. & Masson-Delmotte, V. Bi-hemispheric forcing for Indo-Asian monsoon during glacial terminations. *Quat. Sci. Rev.* **59**, 1–4 (2013).
38. Markle, B. R. et al. Global atmospheric teleconnections during Dansgaard-Oeschger events. *Nat. Geosci.* **10**, 36–40 (2017).
39. Shackleton, S. et al. Global ocean heat content in the Last Interglacial. *Nat. Geosci.* **13**, 77–81 (2020).
40. Holloway, M. D. et al. Antarctic Last Interglacial isotope peak in response to sea ice retreat not ice-sheet collapse. *Nat. Commun.* **7**, 12293 (2016).
41. Ferrari, R. et al. Antarctic sea ice control on ocean circulation in present and glacial climates. *Proc. Natl Acad. Sci. USA* **111**, 8753–8758 (2014).
42. Marzocchi, A. & Jansen, M. F. Connecting Antarctic sea ice to deep-ocean circulation in modern and glacial climate simulations. *Geophys. Res. Lett.* **44**, 6286–6295 (2017).

Publisher's note Springer Nature remains neutral with regard to jurisdictional claims in published maps and institutional affiliations.

© The Author(s), under exclusive licence to Springer Nature Limited 2021

Methods

Analytical measurements. The δD measurements on the EDC ice core at a 55 cm resolution have been performed at Laboratoire des Sciences du Climat et de l'Environnement (LSCÉ) using a uranium reduction method^{43,44}. While the measurements performed over the top part of the ice core and covering the past 420 ka were associated with a 1σ uncertainty of 1‰ , the accuracy was degraded over the deeper part because of analytical issues. This led to artificial scattering of d-excess (Extended Data Fig. 1 and Methods) so that we performed new δD measurements (760 samples) over the deepest part (418 m, covering the period 422 to 800 ka on the AICC2012 timescale^{23,45}) at LSCÉ in 2019–2020 using a Picarro laser spectrometer L2130-i. The uncertainty associated with this new set of measurements is $1\sigma = 0.6\text{‰}$. In parallel, the $\delta^{18}\text{O}$ measurements were performed at University of Parma and Trieste using a water– CO_2 equilibration method with an associated uncertainty of $1\sigma = 0.05\text{‰}$. These measurements were compared with a series of $\delta^{18}\text{O}$ measurements performed with a Picarro laser spectrometer L2130-i at LSCÉ in 2019–2020 over the deepest 418 m of the ice core. The two series of measurements are very similar, with differences smaller than 0.13‰ for 69% of the samples, which should be compared with the $1\sigma = 0.13\text{‰}$ uncertainty for the $\delta^{18}\text{O}$ series of measurements performed with the Picarro L2130-i.

Comparison between d-excess and d_{in} definitions for the EDC, Vostok and Dome F ice cores. The d_{in} definition (in Climate reconstruction of the source evaporative regions) has been chosen to remove nonlinearities in the δD versus $\delta^{18}\text{O}$ relation and d-excess versus $\delta^{18}\text{O}/\delta D$ anticorrelation in the surface snow over East Antarctica¹. However, the δD versus $\delta^{18}\text{O}$ relationship observed in the deep ice-core data is not always similar to the relationship in present-day surface snow and precipitation. In particular, the large d-excess values ($>20\text{‰}$) observed in surface samples are never encountered in deep ice cores¹⁶. Moreover, the EDC data are well aligned on a δD versus $\delta^{18}\text{O}$ linear relationship with a global slope of 8.2 without any important increase of d-excess with decreasing $\delta^{18}\text{O}$ (we rather observe some increase of d-excess with increasing $\delta^{18}\text{O}$). This is slightly different from the δD versus $\delta^{18}\text{O}$ relationships observed in the Dome F and Vostok ice cores, which display a global slope of 7.9 and a slight d-excess anticorrelation to $\delta^{18}\text{O}$ for higher $\delta^{18}\text{O}$ values (Extended Data Fig. 2). Such differences in the isotopic composition of deep ice core versus surface snow are not unexpected. Indeed, d-excess or d_{in} is influenced not only by local temperature but also by the water mass origins and trajectories.

When comparing the $\ln(1 + \delta D)$ versus $\ln(1 + \delta^{18}\text{O})$ relationship of the three ice cores with the $\ln(1 + \delta D)$ versus $\ln(1 + \delta^{18}\text{O})$ relationship found by Uemura et al.²¹ from surface snow isotopic composition, there is a substantial deviation for the EDC ice-core data and to a lesser extent for the Dome F and Vostok data. This is reflected by a positive relationship between d_{in} and $\ln(1 + \delta^{18}\text{O})$ in the deep ice-core data (Extended Data Fig. 2), explaining the strong resemblance between d_{in} and local temperature reconstruction in deep ice cores.

Reconstruction of the T_{site} and T_{source} evolutions. Independently of the 'excess' definitions, efforts were devoted in modelling the isotopic composition (δD and $\delta^{18}\text{O}$) of water vapour and precipitation along a moisture trajectory starting from an oceanic evaporative moisture source toward a precipitation site in Antarctica using the mixed cloud isotopic model (MCIM) adapted to East Antarctica⁴⁷. This model is based on the Rayleigh distillation and has been largely applied to the interpretation of isotopic profiles at Vostok, Dome F and EDC. It takes into account the coexistence of phases between vapour, solid and liquid below 0°C with a description of the Bergeron–Findeisen process and associated water isotopic fractionation. The model contains several parameters (for example, temperature range of coexistence of liquid water and snow, quantity of liquid/snow remaining in the cloud, supersaturation relationship to temperature) that have been tuned to reproduce the evolution of $\delta^{18}\text{O}$ and d-excess in surface snow in Antarctica from the coast to the ice-core drilling sites and, in particular, the observed d-excess increase when $\delta^{18}\text{O}$ decreases below -40‰ . In particular, this MCIM has been tuned and applied to Dome F, Vostok and EDC^{21,26,27} to infer from the $\delta^{18}\text{O}$ and δD variations a scenario for the temperature of final precipitation (T_{site}) as well as for the temperature of the corresponding moisture source (T_{source}). We provide in the following the equations obtained by the different previous studies focused on Vostok, EDC and Dome F^{21,26,27}. The differences in the values of the coefficients between the different sites are due to different tuning of the MCIM by the different authors to best fit the surface values ($\delta^{18}\text{O}$, δD , temperature, pressure) observed at present day over Antarctica.

Vostok²⁶:

$$\Delta T_{source} = 0.07 \times \Delta \delta D + 0.96 \times \Delta d + 2.37 \times \Delta \delta^{18}\text{O}_{sw}$$

$$\Delta T_{site} = 0.5 \times \Delta d + 0.17 \times \Delta \delta D + 0.56 \times \Delta \delta^{18}\text{O}_{sw}$$

EDC²⁷:

$$\Delta T_{source} = 0.06 \times \Delta \delta D_{corr} + 0.93 \times \Delta d_{corr}$$

$$\Delta T_{site} = 0.16 \times \Delta \delta D_{corr} + 0.44 \times \Delta d_{corr}$$

Dome F²¹:

$$\Delta T_{source} = 0.15 \times \Delta \delta D_{corr} + 0.94 \times \Delta d_{corr}$$

$$\Delta T_{site} = 0.19 \times \Delta \delta D_{corr} + 0.39 \times \Delta d_{corr}$$

δD_{corr} , $\delta^{18}\text{O}_{corr}$ and d_{corr} are calculated as:

$$\delta D_{corr} = \delta^{18}\text{O} - \delta^{18}\text{O}_{sw} \times (1 + \delta^{18}\text{O}) / (1 + \delta^{18}\text{O}_{sw})$$

$$\delta D_{corr} = \delta D - 8 \times \delta^{18}\text{O}_{sw} \times (1 + \delta D) / (1 + 8 \times \delta^{18}\text{O}_{sw})$$

$$d_{corr} = \delta D_{corr} - 8 \times \delta^{18}\text{O}_{corr}$$

ΔT_{source} and ΔT_{site} are the differences of temperature between T_{source} and T_{site} at the time of interest and T_{source} and T_{site} at present day (corresponding to the top of the ice core). Δd_{corr} , $\Delta \delta D_{corr}$ and $\Delta \delta^{18}\text{O}_{corr}$ are the differences in d-excess, δD and $\delta^{18}\text{O}$ between the values at the time of interest and the values at the surface (present day) after correction from the effect of $\delta^{18}\text{O}_{sw}$. $\delta^{18}\text{O}_{sw}$ is the global $\delta^{18}\text{O}$ of seawater from the LR04 stack⁴⁹ transferred on the AICC2012 timescale using the correspondence between the LR04 stack and EDC isotopic record⁵⁰.

The uncertainties on the ΔT_{source} and ΔT_{site} reconstructions are given in the original papers. They include uncertainties in the coefficients of the preceding equations (the largest uncertainty being the one associated with the dependency of ΔT_{source} on $\Delta \delta D_{corr}$) and the analytical uncertainties. The resulting uncertainties on the ΔT_{site} and ΔT_{source} values are within 2°C . The reconstructions of ΔT_{source} and ΔT_{site} obtained with the MCIM have been confronted with outputs of more complex modelling approaches (use of general circulation model equipped with water isotopes) and validated for Antarctica. The published comparison⁵¹ between the water isotope-enabled Goddard Institute for Space Studies ModelE-R general circulation model and the MCIM has shown that the d-excess can be used as a faithful tracer of source evaporative conditions, but sensitivity experiments performed with this isotope-enabled general circulation model show that the quantitative relationship between source temperature and d-excess is associated with large uncertainties⁵¹. In fact, much larger uncertainties than those mentioned in the preceding can also arise from the tuning of parameters in the MCIM or general circulation model equipped with water isotopes, especially from the tuning of supersaturation dependency to temperature, which largely increases the uncertainty in the ΔT_{source} reconstruction (by a factor of two)^{21,34}. This is the reason why the interpretation of d-excess in terms of T_{source} should be considered with care.

At Dome F, T_{source} shares many similarities with $\delta^{18}\text{O}$ over deglaciations^{20,21} and is very similar to the d_{in} signal over the glacial–interglacial cycles ($R = 0.97$) but less similar to d-excess ($R = 0.49$). Hence, d_{in} seems a better proxy than d-excess at Dome F to discuss the climatic signal of regions of moisture evaporation. At Vostok, d-excess and T_{source} share more similarities ($R = 0.93$) than d_{in} and T_{source} ($R = 0.78$). The difference between the T_{source} similarities with d-excess or d_{in} among sites is partly due to the way the MCIM has been tuned and to the data selection used for multiple linear correlation²¹. The situation is actually much simpler for EDC, where d-excess, d_{in} and T_{source} are all well correlated (Extended Data Table 1 and Extended Data Figs. 3 and 4), suggesting that the EDC d-excess or d_{in} data are faithful proxies for climatic conditions of associated moisture evaporative regions in East Antarctica over long timescales (several glacial–interglacial cycles).

Extended Data Fig. 4 displays for each termination the evolution of ΔT_{source} , d-excess, d_{in} and $\delta^{18}\text{O}$ or δD (as a proxy for ΔT_{site}). We observe that using any of d-excess, d_{in} or T_{source} at EDC gives exactly the same timing for the maximum during all interglacials. By contrast, there is a very strong shift between the maximum in d_{in} and d-excess for Vostok and Dome F (at Dome F, the d-excess maximum occurs several millennia after the d_{in} maximum), leading to strong variability in the maximum in T_{source} between the different sites. The T_{source} maximum at Dome F is seen in the blue rectangle encompassing the signal of T_{site} maximum while this is not systematically the case at EDC and Vostok. However, we observe that in addition to the first T_{source} maximum occurring in phase with T_{site} at Dome F for interglacials characterized by an excess warmth (early temperature maximum), we often have a T_{source} high value at Dome F and Vostok at the timing of the EDC d-excess/ T_{source} maximum over the different interglacial periods.

Given these observations, we conclude that we have not enough evidence to say that the climatic evolutions of the source evaporative regions are different at Dome F, Vostok and EDC over terminations and interglacial periods. We thus propose that the pattern reconstructed from the water isotopic record at EDC can be taken as a good first-order pattern to describe the climatic evolution of the source evaporative regions for East Antarctica.

Modelling d-excess with ECHAM6-wiso. With the objective to discuss differences between Dome C, Vostok and Dome F, we used the ECHAM6-wiso model³² outputs from a free simulation at T63L47 spatial resolution (1.875° horizontal resolution and 47 atmosphere vertical layers) based on pre-industrial conditions: mean 1870–1899 Atmospheric Model Intercomparison Project sea surface temperature and sea-ice boundary conditions, orbital and greenhouse gas conditions according to Paleoclimate Model Intercomparison Project phase 4 PI experimental design and isotopic composition of surface seawater prescribed using the adapted global gridded dataset⁵². This ECHAM6-wiso simulation provides a good representation of the Marshall SAM calculated as the difference in pressure at sea level between latitudes 40°S and 65°S (ref. 53). The simulated SAM has a similar average (0), similar normalized standard deviation (1.88 versus 1.74) and similar frequency as the station-based index of SAM³⁰ as shown in Extended Data Figs. 5 and 6. Moreover, the correlation maps between SAM and surface temperature or precipitation from ERA-Interim data⁵¹ are very similar when considering the data and the model (Extended Data Fig. 7 and 8). The simulated correlations between SAM and d-excess or d_{in} are displayed in Fig. 1 and Extended Data Fig. 9.

Data availability

The data associated with this study were posted on the PANGAEA database under the following link: <https://doi.org/10.1594/PANGAEA.934094>.

Code availability

The ECHAM model code is available under a version of the MPI-M software license agreement (<https://www.mpimet.mpg.de/en/science/models/license/>). The code of the isotopic version ECHAM6-wiso is available upon request on the AWTs GitLab repository (<https://gitlab.awi.de/mwerner/mpe-esm-wiso>).

References

43. Vaughn, B. H. et al. An automated system for hydrogen isotope analysis of water. *Chem. Geol.* **152**, 309–319 (1998).
44. Jouzel, J. et al. Orbital and millennial Antarctic climate variability over the past 800,000 years. *Science* **317**, 793–796 (2007).
45. Veres, D. et al. The Antarctic ice core chronology (AICC2012): an optimized multi-parameter and multi-site dating approach for the last 120 thousand years. *Clim. Past* **9**, 1733–1748 (2013).
46. Pang, H. et al. Spatial distribution of ^{17}O -excess in surface snow along a traverse from Zhongshan station to Dome A, East Antarctica. *Earth Planet. Sci. Lett.* **414**, 126–133 (2015).
47. Ciais, P. & Jouzel, J. Deuterium and oxygen 18 in precipitation: isotopic model, including mixed cloud processes. *J. Geophys. Res. Atmos.* **99**, 16793–16803 (1994).
48. Jouzel, J. et al. Magnitude of isotope/temperature scaling for interpretation of central Antarctic ice cores. *J. Geophys. Res. Atmos.* <https://doi.org/10.1029/2002JD002677> (2003).
49. Lisiecki, L. E. & Raymo, M. E. A Pliocene–Pleistocene stack of 57 globally distributed benthic $\delta^{18}\text{O}$ records. *Paleoceanogr. Paleoclimatol.* <https://doi.org/10.1029/2004PA001071> (2005).
50. Parrenin, F. et al. The EDC3 chronology for the EPICA Dome C ice core. *Clim. Past* **3**, 485–497 (2007).
51. Lewis, S. C., LeGrande, A. N., Kelley, M. & Schmidt, G. A. Modeling insights into deuterium excess as an indicator of water vapor source conditions. *J. Geophys. Res. Atmos.* **118**, 243–262 (2013).
52. LeGrande, A. N. & Schmidt, G. A. Global gridded data set of the oxygen isotopic composition in seawater. *Geophys. Res. Lett.* <https://doi.org/10.1029/2006GL026011> (2006).
53. Marshall, G. J. Trends in the Southern Annular Mode from observations and reanalyses. *J. Clim.* **16**, 4134–4143 (2003).
54. Dee, D. P. et al. The ERA-Interim reanalysis: configuration and performance of the data assimilation system. *Q. J. R. Meteorol. Soc.* **137**, 553–597 (2011).

Acknowledgements

This work is a contribution to EPICA, a joint European Science Foundation/European Commission (EU) scientific programme, funded by the European Union and by national contributions from Belgium, Denmark, France, Germany, Italy, the Netherlands, Norway, Sweden, Switzerland and the United Kingdom. The main logistic support was provided by Institut Polaire Français Paul-Emile Victor and Programma Nazionale Ricerche in Antartide (at Dome C) and Alfred Wegener Institute (at Dronning Maud Land). We thank the Dome C logistics teams and the drilling team that made the science possible. The research leading to these results has also received funding from the European Research Council under the European Union H2020 Programme (H2020/20192024)/ERC grant agreement no. 817493 ERC ICORDA (A.L., E.F.). We thank E. Michel for useful comments on the manuscript. This study is also part of the project ANR NEANDROOT.

Author contributions

A.L., B.S., J.J. and V.M.-D. designed the study. B.S., E.S., B.M. and A.G. performed the measurements. A.C., M.W. and T.E. worked on the modelling aspects. A.L. led the data analyses and the writing of the manuscript with the active contribution of all co-authors.

Competing interests

The authors declare no competing interests.

Additional information

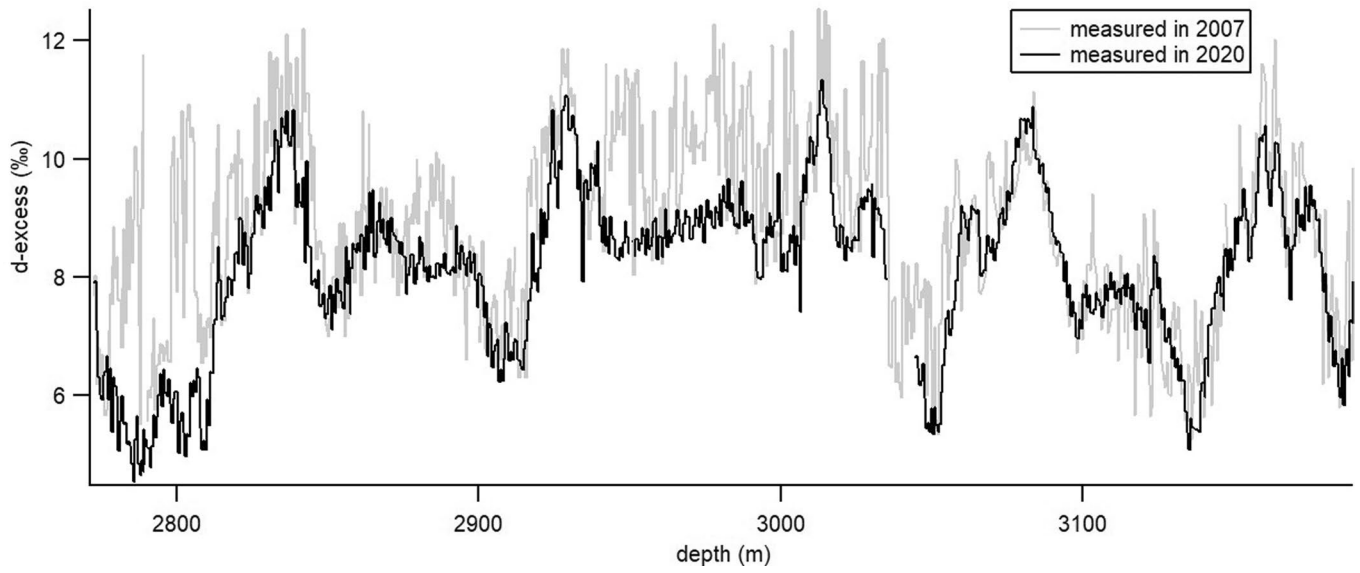
Extended data is available for this paper at <https://doi.org/10.1038/s41561-021-00856-4>.

Supplementary information The online version contains supplementary material available at <https://doi.org/10.1038/s41561-021-00856-4>.

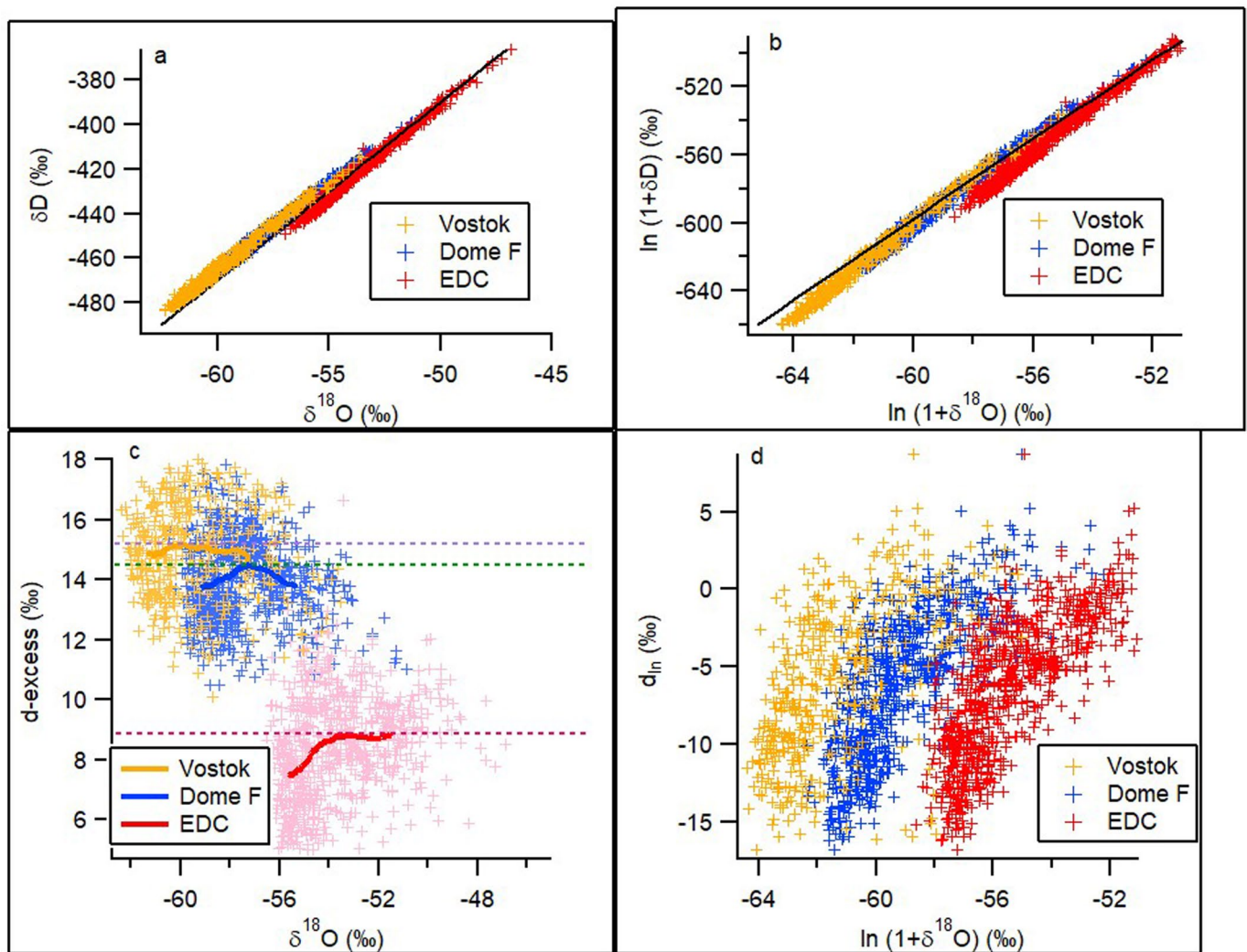
Correspondence and requests for materials should be addressed to A. Landais.

Peer review information *Nature Geoscience* thanks Daniel Lowry, Ben Kopec and the other, anonymous, reviewer(s) for their contribution to the peer review of this work. Primary Handling Editor: James Super.

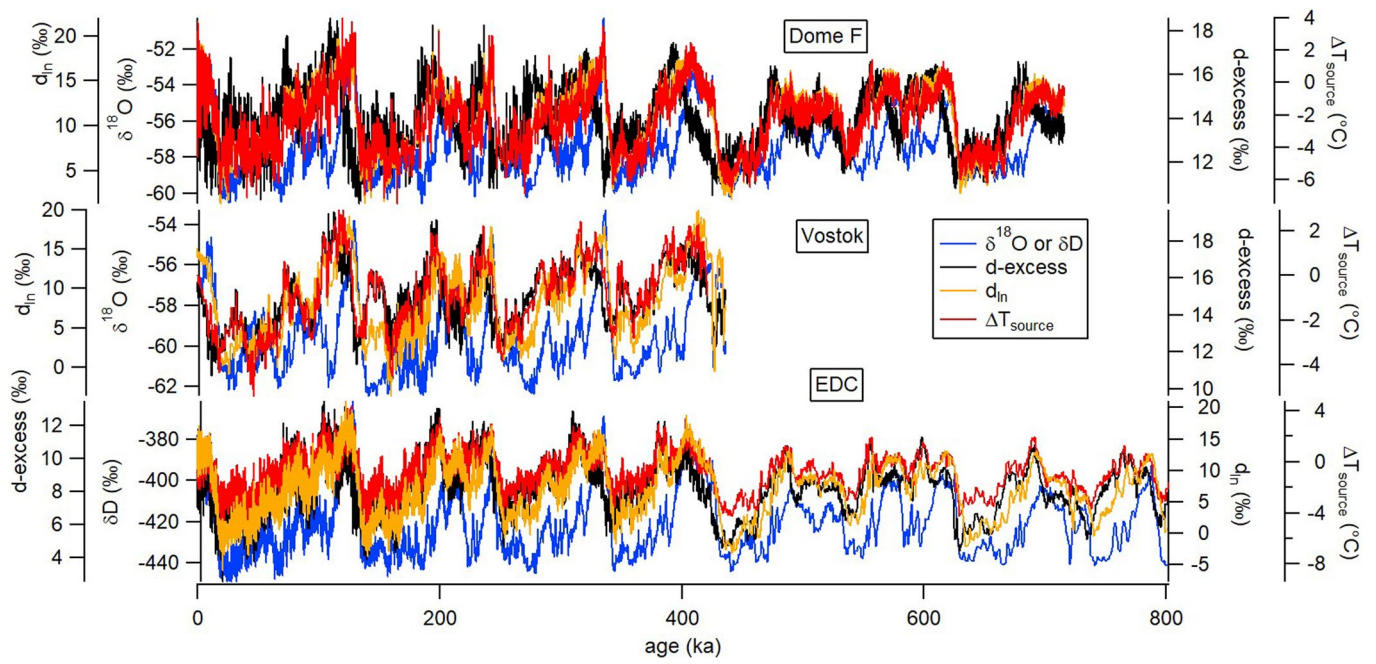
Reprints and permissions information is available at www.nature.com/reprints.



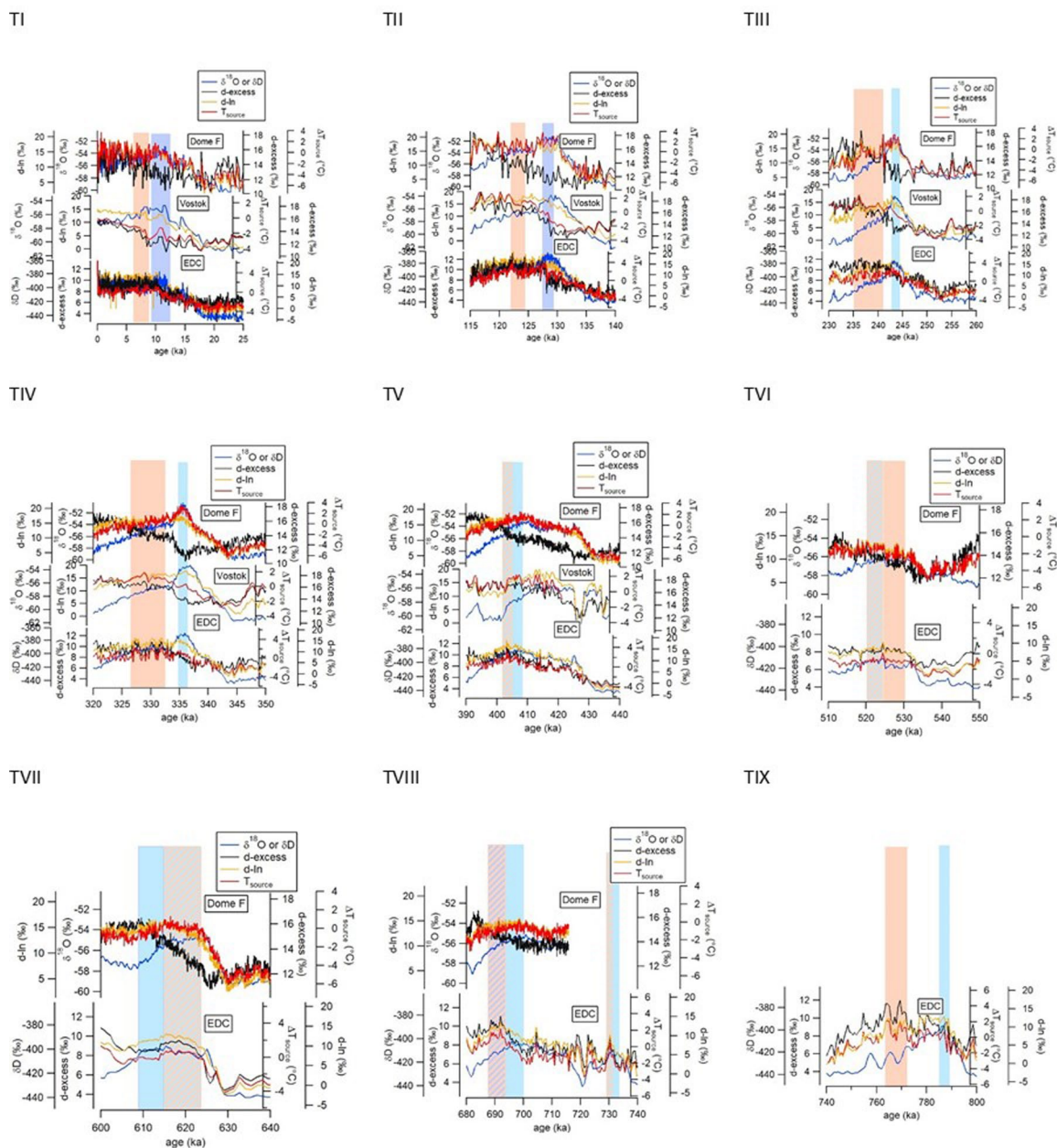
Extended Data Fig. 1 | Raw d-excess data. Comparison between d-excess calculated with initial δD data measured in 2007 (grey) and d-excess calculated with new δD data measured in 2020 (black).



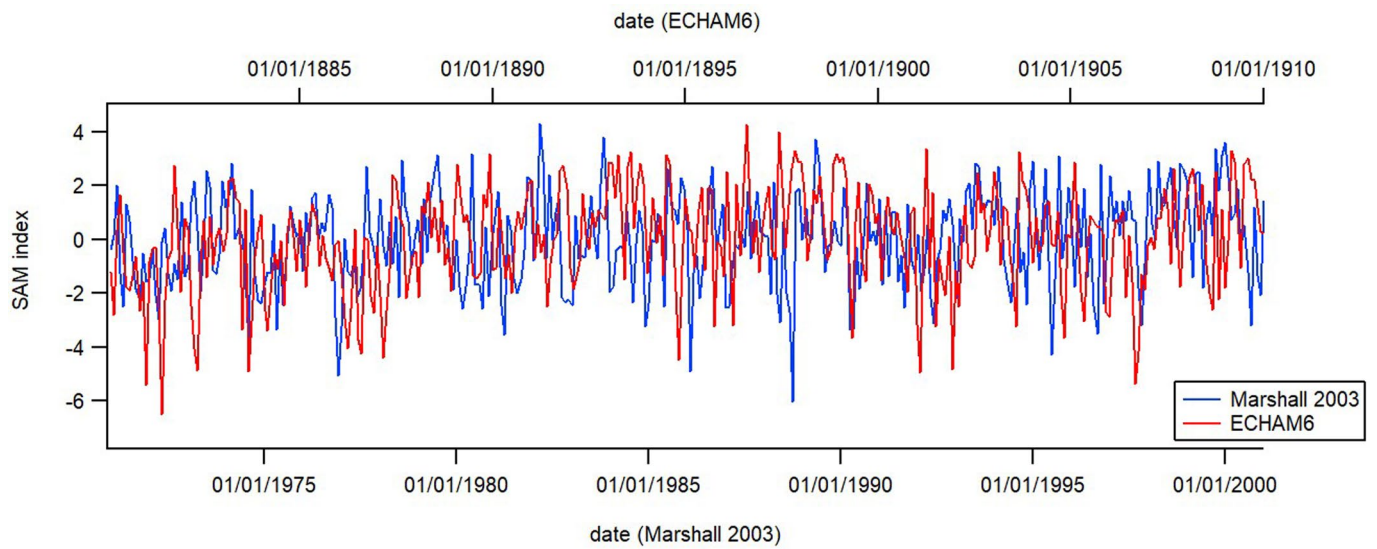
Extended Data Fig. 2 | Evolution of the isotopic composition (a: δD vs $\delta^{18}O$, b: $\ln(1+\delta D)$ vs $\ln(1+\delta^{18}O)$, c: d-excess vs $\delta^{18}O$, d: d_{in} vs $\ln(1+\delta^{18}O)$) for the three deep ice cores of the East Antarctic plateau (red - EDC; blue - Dome F; orange - Vostok). The black line on panel a represents the Global Meteoric Water Line, a linear relationship between δD and $\delta^{18}O$ with a slope of 8 (and intercept of 10 ‰). The black line on panel b represents the ln regression determined from surface snow samples by Uemura et al. (2012)¹. The solid lines on panel c represent the evolution of d-excess vs $\delta^{18}O$ after a running mean over a 2‰ wide window on the $\delta^{18}O$ scale, and the dashed lines represent the average d-excess value.



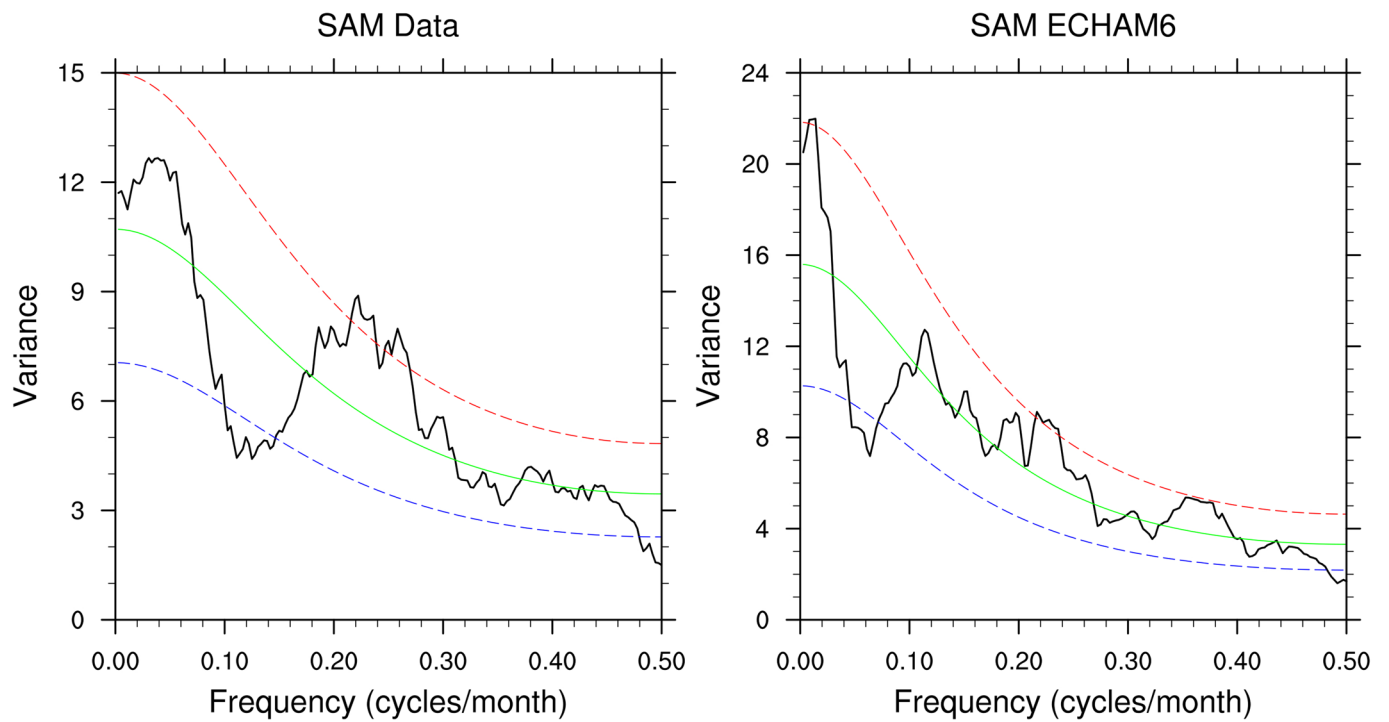
Extended Data Fig. 3 | Isotopic records on three deep drilling sites of the East Antarctic plateau. Comparison of $\delta^{18}\text{O}$ or δD , d-excess, d_{in} and ΔT_{source} for the three sites of interest Dome F, Vostok and EDC.



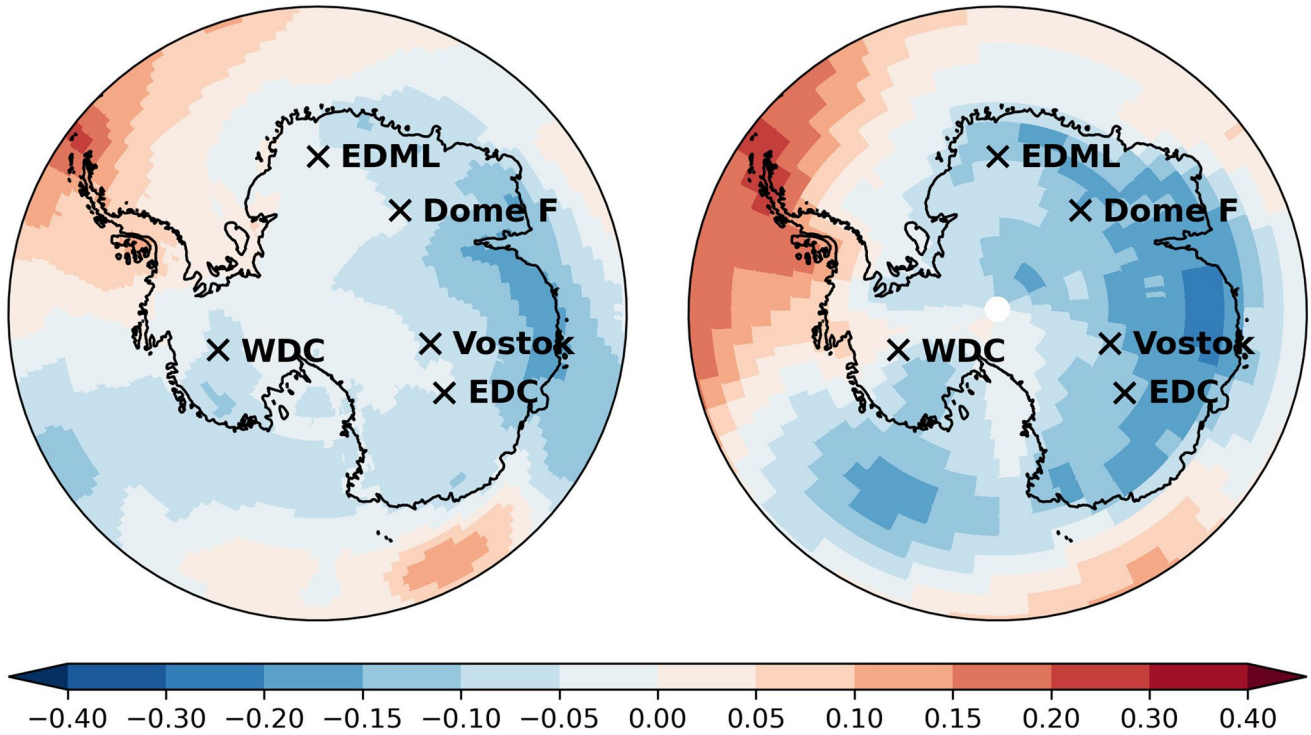
Extended Data Fig. 4 | Evolution of $\delta^{18}\text{O}$ or δD in blue, d-excess in black, d_{in} in yellow and ΔT_{source} in red, over the last 9 terminations for each site considered in the text, Vostok, Dome F and EDC, all on the AICC2012 timescale. The blue and orange rectangles correspond to those defined in Fig. 4 of the main text, highlighting maxima in T_{site} and d-excess at EDC. Note that the Vostok records could not be well aligned on the AICC2012 timescale over Termination V because of lack of relative dating constraints so that the comparison of Vostok to other sites over Termination V is not meaningful.



Extended Data Fig. 5 | Model-data comparison of the SAM variability. Comparison of the SAM variability as inferred from observations and reanalyses between 1971 and 2000 and as inferred from the ECHAM6—wiso model free simulation for pre-industrial period.

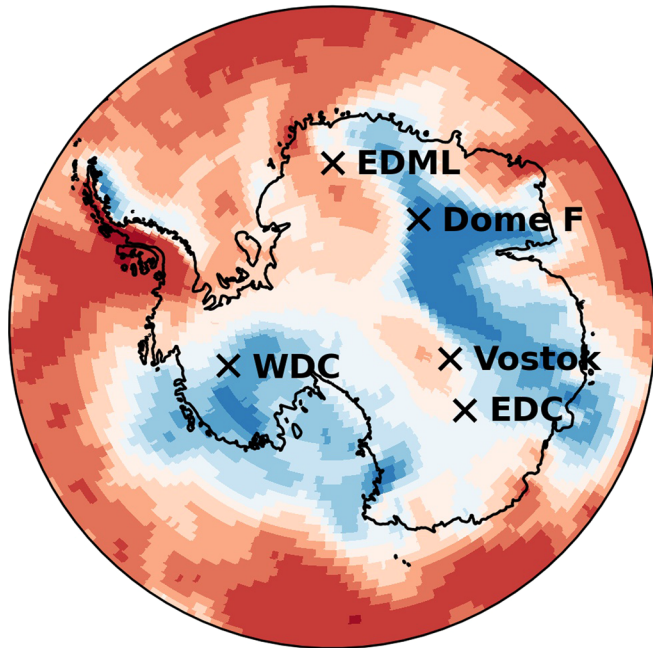


Extended Data Fig. 6 | Spectral analysis of the SAM variability from the Marshall series (left) and from the ECHAM6-wiso model (right). In both cases, we see a peak at 0.22 month^{-1} .

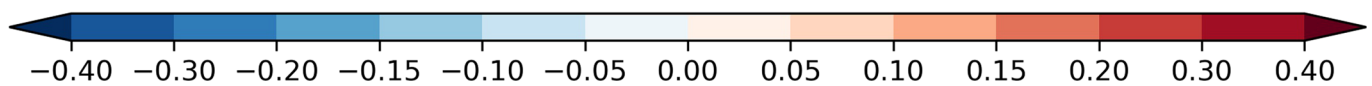
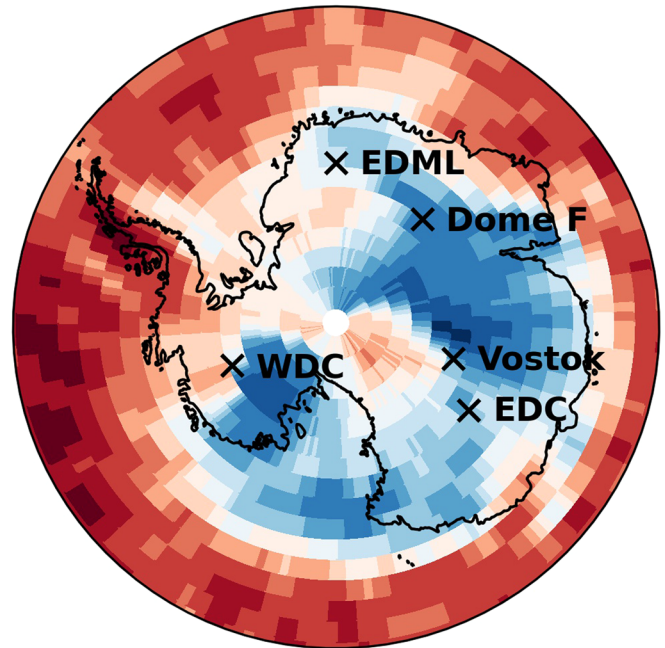
(a) Observed SAM – T_{2m}
correlation(b) ECHAM6-wiso SAM – T_{2m}
correlation

Extended Data Fig. 7 | SAM vs temperature correlation. Map of the correlation between SAM and 2-m temperature (T_{2m}) from the ERA-Interim data (a) and from the ECHAM6-wiso free simulation (b).

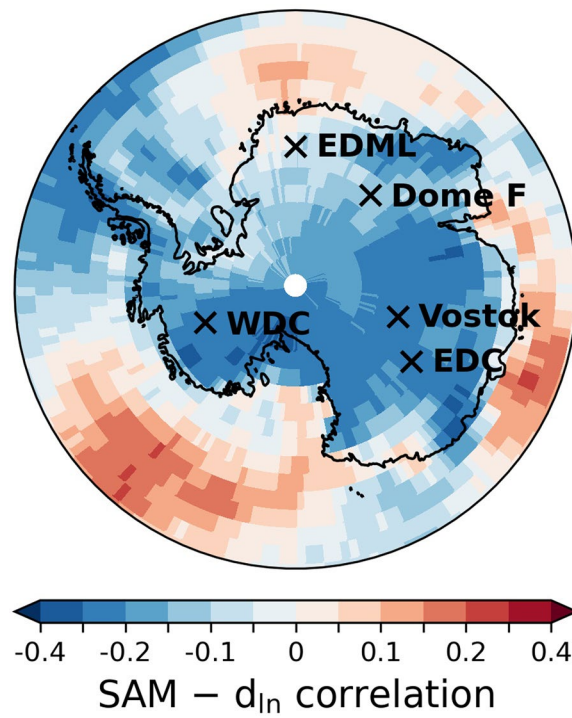
(a) Observed SAM – P correlation



(b) ECHAM6-wiso SAM – P correlation



Extended Data Fig. 8 | SAM vs pressure correlation. Map of the correlation between SAM and precipitation from the ERA- Interim data (a) and from the ECHAM6-wiso free simulation (b).



Extended Data Fig. 9 | d_{in} vs SAM correlation. Modelled correlation between d_{in} and SAM as obtained from the ECHAM6-wiso model for a pre-industrial run.

Extended Data Table 1 | Correlation coefficients between d-excess, d_{in} and T_{source} for the three East Antarctic ice cores EDC, Vostok and Dome F

		d_{in}	T_{source}
EDC	d-excess	0.80	0.93
	d_{in}	1	0.93
Vostok	d-excess	0.59	0.93
	d_{in}	1	0.78
Dome F	d-excess	0.59	0.49
	d_{in}	1	0.97